

Learning to Beamform for Cooperative Localization and Communication: A Link Heterogeneous GNN-Based Approach

Lixiang Lian, *Member, IEEE*, Chuanqi Bai, Yihan Xu, Huanyu Dong, Rui Cheng and Shunqing Zhang, *Senior Member, IEEE*

Abstract—Integrated sensing and communication (ISAC) has emerged as a key enabler for next-generation wireless networks, supporting advanced applications such as high-precision localization and environment reconstruction. Cooperative ISAC (CoISAC) further enhances these capabilities by enabling multiple base stations (BSs) to jointly optimize communication and sensing performance through coordination. However, CoISAC beamforming design faces significant challenges due to system heterogeneity, large-scale problem complexity, and sensitivity to parameter estimation errors. Traditional deep learning-based techniques fail to exploit the unique structural characteristics of CoISAC systems, thereby limiting their ability to enhance system performance. To address these challenges, we propose a Link-Heterogeneous Graph Neural Network (LHGNN) for joint beamforming in CoISAC systems. Unlike conventional approaches, LHGNN models communication and sensing links as heterogeneous nodes and their interactions as edges, enabling the capture of the heterogeneous nature and intricate interactions of CoISAC systems. Furthermore, a graph attention mechanism is incorporated to dynamically adjust node and link importance, improving robustness to channel and position estimation errors. Numerical results demonstrate that the proposed attention-enhanced LHGNN achieves superior communication rates while maintaining sensing accuracy under power constraints. The proposed method also exhibits strong robustness to communication channel and position estimation error.

Index Terms—Cooperative ISAC, direct localization, beamforming, heterogeneous graph neural networks.

I. INTRODUCTION

INTEGRATED sensing and communication (ISAC) has become a key technology in next-generation wireless communication networks. By integrating the sensing and communication functionalities, the ISAC system can support various cutting-edge applications such as high-precision localization, environment reconstruction, smart healthcare, etc[1]. Utilizing the same spectrum and hardware resources, one of the key issues of ISAC is to guarantee both sensing and communication performance. Cooperative ISAC (CoISAC) has drawn much attention due to its potential to enhance both communication

and sensing services. By connecting to a common central processing unit (CPU), multiple base stations (BSs) cooperatively provide joint communication and sensing services. Coordination among BSs can better manage the interferences among communication users to improve the communication data rate. Additionally, multiple BSs provide diverse spatial information, enhancing the precision of sensing tasks. By combining information from various sources relying on the widely-used cloud radio access network (C-RAN) architecture [2], CoISAC enhances efficiency and robustness for both communication and sensing tasks[3].

Despite the potential benefits of CoISAC, the design of a joint beamforming scheme for multi-BS CoISAC systems to simultaneously optimize multi-user communication performance and target sensing performance presents significant challenges. First, CoISAC system exhibits significant heterogeneity across multiple dimensions. Communication and sensing functions differ in optimization objectives, link characteristics, and signal responses, for communication users and sensing targets. Moreover, when multiple BSs collaborate, heterogeneity arises among BSs in terms of varying resource budgets, physical environments, and channel conditions associated with communication and sensing users. The system's multi-objective nature and complex link topology significantly increase the complexity of the joint beamforming problem. Second, the shift towards 6G technology results in an expanded problem scale due to the increased number of antennas, higher network density, and the cooperation among multiple BSs. This, in turn, leads to a significantly larger-scale transmit beamforming design problem in CoISAC systems. Third, accurate channel information in communication and precise target information in sensing are essential for directing beamforming design. Errors in estimation can lead to misdirected beams, thereby degrading both communication and sensing performance [4]. Therefore, designing beamforming schemes that are robust to estimation errors in CoISAC systems is of great importance, which, however, can induce additional complexities.

To address these difficulties, previous works mainly utilize traditional optimization-based algorithms for beamforming design. [5] investigated the joint waveform design and BS clustering problem in CoISAC, considering sensing performance, communication performance, and the backhaul capacity limitation. Fractional programming (FP) techniques such as Dinkel-bach's transform and quadratic transform are adopted

Lixiang Lian, Chuanqi Bai, Yihan Xu and Huanyu Dong are with the School of Information Science and Technology, ShanghaiTech University, Shanghai 201210, China (e-mail: lianlx@shanghaitech.edu.cn; baichq2024@shanghaitech.edu.cn; xuyh3@shanghaitech.edu.cn; huanyu.dong0425@gmail.com).

Rui Cheng and Shunqing Zhang are with the Shanghai Institute for Advanced Communication and Data Science, Key Laboratory of Specialty Fiber Optics and Optical Access Networks, School of Information and Communication Engineering, Shanghai University, Shanghai, 200444, China (e-mail: cora_cheng@shu.edu.cn; shunqing@shu.edu.cn).

to tackle the fractional signal-to-interference-plus-noise ratio (SINR) objectives. Successive convex approximation (SCA) and semidefinite relaxation (SDR) are utilized to handle the non-convexity of the clustering and beamforming, respectively. [6] studied the minimization of the angular parameter Cramér-Rao bound (CRB) in mono-static and bi-static CoISAC scenarios. FP and SDR are also adopted to convexify the beamforming design problem. [7] investigated CoISAC beamforming design considering squared position error bound (SPEB) and communication rate requirements. SCA technique is adopted to tackle the non-convexity of BS scheduling, fronthaul, and SPEB constraints. However, these traditional methods have several drawbacks. First, traditional algorithms handle the non-convexity of the optimization problem using approximation methods, such as SCA, FP, and SDR, which can only derive sub-optimal solutions. Second, traditional algorithms usually need to iterate until they converge, and also involve high-complexity operations such as matrix inversion and decomposition. Thus, traditional algorithms usually have high complexity and poor scalability, causing extremely high computational latency. Third, although robust beamforming design has been considered in ISAC systems, such as [8], [9], to handle information uncertainties, the resulting optimization algorithms are extremely complex, and not well-suited for practical systems. In addition to their complexities, these works rely on uncertainty sets of parameters defined by specific thresholds. This inflexibility can lead to either overly pessimistic or overly optimistic solutions.

Deep learning has attracted a lot of attention in physical layer optimization due to its excellent approximation capability and low inference complexity. A lot of works have investigated deep learning-based ISAC beamforming design. [10] proposed a convolutional long short-term memory (LSTM) network-based algorithm to extract the features of historical channels and predict the ISAC beamforming in the vehicle networks, which reduces the dependency on real-time CSI. [11] proposed a deep reinforcement learning-based algorithm to solve the radar beam pattern error-constrained sum-rate maximization problem in an intelligent reflecting surface (IRS)-aided ISAC scenario. [12] studied deep learning-based ISAC beamforming algorithm, aimed at maximizing the average SINR for multi-user communication while guaranteeing the detection probability of radar targets. [13] investigated the joint sensing transmit waveform and communication receive beamforming design with the objective of maximizing the weighted sum of the normalized sensing rate and normalized communication rate in an uplink scenario leveraging the deep learning techniques. However, current deep learning-based ISAC systems primarily employ general-purpose neural networks, such as convolutional neural networks (CNNs) [14], LSTMs [10], or feedforward neural networks (FNNs) [15], for beamforming design, without leveraging the specific network topology of ISAC systems. In particular, considering the heterogeneous nature of the CoISAC system's network topology and the optimization problem itself, directly applying these general-purpose neural networks to CoISAC for beamforming design faces several challenges [16]. First, the training efficiency is low, severely impacting learning performance. Second, the

scalability and generalizability of these networks are poor, making them unsuitable for large-scale CoISAC topologies. Therefore, developing specialized neural networks tailored to beamforming optimization in CoISAC systems is essential.

Graph neural networks (GNN) can effectively incorporate graph structures, modeling node attributes and relationships between nodes to explore hidden features in graph-structured data [17]. Therefore, GNNs have been introduced to solve a broad range of optimization problems in wireless networks, such as multi-user beamforming problem in cell-free networks [18], joint sensing and communication service scheduling and vehicle association in vehicular networks [19], joint Sub-6G and mmWave networks [20], etc. By exploiting the inherent property of the problem, GNN can achieve near-optimal performance with faster training speed, fewer training samples, better scalability and generalizability than general-purpose networks [16]. However, to the best of our knowledge, there are no previous works focused on CoISAC beamforming optimization based on GNN. Due to the heterogeneity in CoISAC systems, traditional bipartite graph modeling cannot adequately represent the complex link structures and multi-objective nature of the network. To effectively model the heterogeneous link types and their complex interaction in CoISAC systems, a link-heterogeneous GNN (LHGNN) will be proposed in this paper. Instead of modeling each device as a heterogeneous node, we model the different types of links, such as communication and sensing links that connect multiple ISAC-enabled BSs with multiple communication users and sensing target, as heterogeneous nodes. This approach allows us to construct a link-node-based graph structure, which fully capture the heterogeneous nature and intricate interactions of CoISAC systems. To improve the robustness of the LHGNN to parameter estimation errors, we further incorporate a graph attention mechanism into LHGNN. This enables the GNN to learn the optimal weights during the information aggregation, adapting to the input parameter errors and thereby reducing the impact of parameter uncertainties on the final beamforming output.

In this paper, we focus on the scenario of multi-BS collaborative localization and communication, innovatively introducing LHGNN for beamforming design in CoISAC systems. Graph attention is adopted to improve the robustness to channel and target position estimation errors. Our main contributions are summarized as follows:

- **Link-Heterogeneous GNN Network for Joint Beamforming in CoISAC Systems:** We consider multi-BSs are collaboratively supporting multi-user communication and target direct localization simultaneously. We derive the squared position error bound (SPEB) performance metric in CoISAC systems to characterize the direct localization error. Then an SPEB and power constrained sum-rate maximization problem is formulated to jointly design the communication and sensing beamforming vectors at multiple BSs. To fully capture the heterogeneity of CoISAC networks, we model the different types of links as heterogeneous nodes and interferences among links as edges to construct the graph. Compared to the traditional bipartite graph model, the proposed LHGNN effectively

models the heterogeneous structure of communication and sensing links and fully exploiting the dependencies between different nodes.

- **Graph Attention Mechanism-Enhanced LHGNN for Improved Robustness:** We introduce the graph attention mechanism into the LHGNN to enhance its robustness to errors in communication channels and position estimation. This mechanism allows the model to dynamically adjust the importance of different nodes and links, effectively mitigating the impact of inaccurate input information on the final beamforming outputs and improving the robustness of CoISAC systems in the presence of parameter uncertainties.
- Numerical results have demonstrated that the proposed attention-enhanced LHGNN achieves better performance in terms of achievable communication rate while ensuring sensing performance and power consumption. Additionally, the proposed algorithm has exhibited good robustness to channel and position estimation errors.

The rest of paper is organized as follows. In Section II, we present the signal models of CoISAC systems, derive the squared position error bound for cooperative localization, and formulate the joint beamforming optimization problem. In Section III, we propose the framework of LHGNN, as well as the graph attention mechanism to effectively solve the joint beamforming problem in CoISAC systems. Finally, the extensive simulation results are provided in Section IV and conclusions are drawn in Section V.

II. SYSTEM MODEL

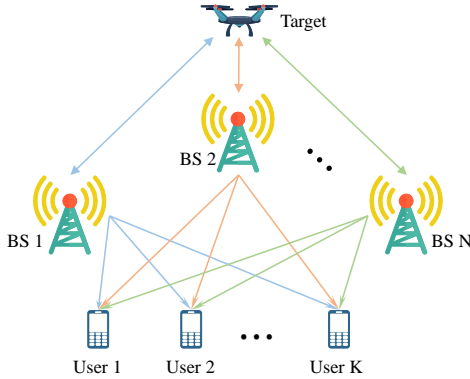


Fig. 1. Illustration of the proposed cooperative ISAC system.

In this section, we investigate a CoISAC system involving multiple dual-functional BSs and multiple users, which is illustrated in Fig. 1. In particular, N BSs cooperatively serve K single-antenna downlink users, while estimating the position of a single sensing target¹. Each BS has a uniform planar array (UPA) with L antenna elements. The BSs are connected to a central processor (CP) through ideal backhaul links. The transmit data assignment and precoding matrices

¹Although a single target is considered during the problem formulation, the proposed algorithm can be readily extended to multiple sensing targets scenario by including multiple sensing links.

design are conducted at the CP and then distributed to each BS via fronthaul links. $\mathcal{N} = \{1, \dots, N\}$ and $\mathcal{K} = \{1, \dots, K\}$ denote the indices of BSs and users, respectively.

A. Communication Model

Each BS transmits symbols $\mathbf{s} = [s^s, s_1^c, \dots, s_K^c]^T$, where s_k^c denotes the symbol for the k -th downlink user from BS and s^s is the dedicated symbol for target sensing. We consider all symbols to be unit-power and independent from each other, i.e., $\mathbb{E}[\mathbf{s}\mathbf{s}^H] = \mathbf{I}_{K+1}$. The transmit signal of the n -th BS can be formulated as

$$\mathbf{x}_n = \mathbf{P}_n \mathbf{s} = \mathbf{p}_n^s s^s + \sum_{k=1}^K \mathbf{p}_{n,k}^c s_k^c, \quad (1)$$

where $\mathbf{P}_n = [\mathbf{p}_n^s, \mathbf{p}_{n,1}^c, \dots, \mathbf{p}_{n,K}^c] \in \mathbb{C}^{L \times (K+1)}$. Denote $\mathbf{p}^s = [\mathbf{p}_1^{s,T}, \dots, \mathbf{p}_N^{s,T}]^T \in \mathbb{C}^{NL \times 1}$ as the coordinated sensing beamforming vectors of N BSs, $\mathbf{p}_k^c = [\mathbf{p}_{1,k}^{c,T}, \dots, \mathbf{p}_{N,k}^{c,T}]^T \in \mathbb{C}^{NL \times 1}$ as the coordinated communication beamforming vectors of N BSs for the k -th user, and $\mathbf{x} = [\mathbf{x}_1^T, \dots, \mathbf{x}_N^T]^T \in \mathbb{C}^{NL \times 1}$ as the concatenated transmit signal of N BSs, respectively. Then the received signal of the k -th user is formulated as

$$\begin{aligned} y_k &= \mathbf{h}_k^H \mathbf{x} + n_k \\ &= \mathbf{h}_k^H \mathbf{p}_k^c s_k^c + \left(\mathbf{h}_k^H \mathbf{p}^s s^s + \sum_{j \in \mathcal{K}, j \neq k} \mathbf{h}_k^H \mathbf{p}_j^c s_j^c \right) + n_k, \end{aligned} \quad (2)$$

where $\mathbf{h}_k = [\mathbf{h}_{k,1}^H, \mathbf{h}_{k,2}^H, \dots, \mathbf{h}_{k,N}^H]^H \in \mathbb{C}^{NL \times 1}$ is the concatenated channel vector between N BSs and the k -th user. Without loss of generality, we consider $n_k \sim \mathcal{CN}(0, \sigma^2)$ is the complex additive white Gaussian noise with zero mean and variance σ^2 . Then the communication SINR can be expressed as

$$\text{SINR}_k = \frac{|\mathbf{h}_k^H \mathbf{p}_k^c|^2}{|\mathbf{h}_k^H \mathbf{p}^s|^2 + \sum_{j \in \mathcal{K}, j \neq k} |\mathbf{h}_k^H \mathbf{p}_j^c|^2 + \sigma^2}. \quad (3)$$

According to (3), the achievable communication rate of user k is given by

$$R_k = \log_2(1 + \text{SINR}_k). \quad (4)$$

B. Sensing Model

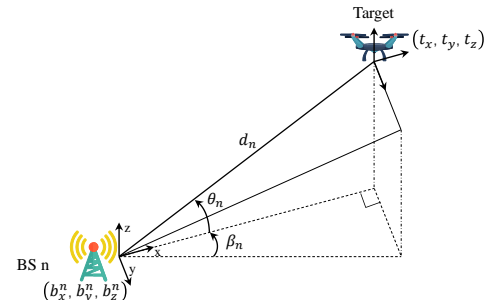


Fig. 2. Illustration of the geometric relationship between the sensing target and a BS.

Before diving into the signal model for target localization, we first introduce the geometric settings. Let Cartesian coordinates $\mathbf{t} = [t_x, t_y, t_z]^T$ and $\mathbf{b}^n = [b_x^n, b_y^n, b_z^n]^T$ represent the position of the sensing target and the position of the n -th BS, respectively. We assume all BSs are with same height and placed onto the same plane. As described in Fig. 2, the elevation and azimuth angle of the target corresponding to the n -th BS are denoted by $\theta_n \in [-\pi/2, \pi/2]$ and $\beta_n \in [-\pi, \pi]$, respectively. Thus, the elevation angle θ_n can be expressed as

$$\theta_n = \arcsin \frac{t_z - b_z^n}{d_n}, \quad (5)$$

where $d_n = \sqrt{(t_x - b_x^n)^2 + (t_y - b_y^n)^2 + (t_z - b_z^n)^2}$ denotes the Euclidean distance between the n -th BS and the sensing target. The azimuth angle β_n can be expressed as

$$\beta_n = \arctan \frac{t_y - b_y^n}{t_x - b_x^n} + \pi \cdot 1(t_x < b_x^n). \quad (6)$$

If $t_x < b_x^n$, then $1(\cdot)$ equals to 1, otherwise 0.

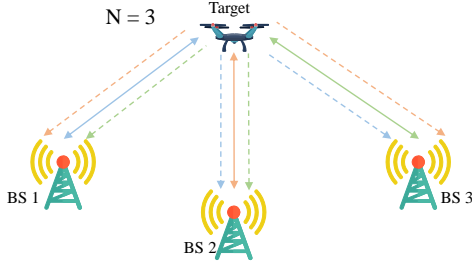


Fig. 3. Cooperative localization between multiple base stations.

As shown in Fig. 3, we consider that all BSs have line-of-sight (LoS) links to the sensing target. As a result, the received echo at the n -th BS contains the reflected signal of all BSs by the target, which is given by

$$\begin{aligned} \mathbf{y}_n &= \sum_{m=1}^N \mathbf{H}_{m,n} \mathbf{x}_m + \mathbf{n}_n \\ &= \sum_{m=1}^N \alpha_{m,n} \mathbf{a}_r(\theta_n, \beta_n) \mathbf{a}_t^H(\theta_m, \beta_m) \mathbf{P}_m \mathbf{s} + \mathbf{n}_n, \end{aligned} \quad (7)$$

where $\mathbf{H}_{m,n}$ is the sensing channel response matrix with respect to the m -th transmit BS and the n -th receiving BS, $\alpha_{m,n}$ is the corresponding reflection coefficient, and $\mathbf{n}_n \sim \mathcal{CN}(0, \sigma_n^2 \mathbf{I}_L)$ is the complex Gaussian noise. For simplicity, we consider the BSs share a common noise level, i.e., $\sigma_n^2 = \sigma^2$. Assume the UPA at BS is placed on the x - z plane with the size $L_x \times L_z$. The transmit steering vector $\mathbf{a}_t(\theta_n, \beta_n) \in \mathbb{C}^{L \times 1}$ and the receive steering vector $\mathbf{a}_r(\theta_n, \beta_n) \in \mathbb{C}^{L \times 1}$ of a UPA can be expressed as

$$\begin{aligned} \mathbf{a}(\theta_n, \beta_n) &= \frac{1}{\sqrt{L}} \left[1, \dots, e^{j \frac{2\pi}{\lambda} d(i_x \cos \beta_n \cos \theta_n + i_z \sin \theta_n)}, \right. \\ &\quad \left. \dots, e^{j \frac{2\pi}{\lambda} d((L_x - 1) \cos \beta_n \cos \theta_n + (L_z - 1) \sin \theta_n)} \right]^T, \end{aligned} \quad (8)$$

where d is the antenna spacing, λ is the signal wavelength, $i_x \in \{1, \dots, L_x - 1\}$ and $i_z \in \{1, \dots, L_z - 1\}$ are the

antenna indices along the x coordinate and z coordinate. By reformulating eq.(7) into a matrix form, we derive

$$\mathbf{y}_n = \mathbf{a}_r(\theta_n, \beta_n) \mathbf{A}_t(\boldsymbol{\theta}, \boldsymbol{\beta}) \mathbf{B}(\boldsymbol{\alpha}_n) \mathbf{P} \mathbf{s} + \mathbf{n}_n, \quad (9)$$

where

$$\mathbf{A}_t(\boldsymbol{\theta}, \boldsymbol{\beta}) = [\mathbf{a}_t^H(\theta_1, \beta_1), \dots, \mathbf{a}_t^H(\theta_N, \beta_N)] \in \mathbb{C}^{1 \times NL}, \quad (10)$$

$$\mathbf{B}(\boldsymbol{\alpha}_n) = \text{Diag}(\boldsymbol{\alpha}_n) \otimes \mathbf{I}_L \in \mathbb{C}^{NL \times NL}, \quad (11)$$

$$\mathbf{P} = [\mathbf{P}_1^H, \dots, \mathbf{P}_N^H]^H \in \mathbb{C}^{NL \times (K+1)}, \quad (12)$$

$$\boldsymbol{\alpha}_n = [\alpha_{1,n}, \dots, \alpha_{K,n}]^T, \quad (13)$$

$$\boldsymbol{\theta} = [\theta_1, \dots, \theta_N]^T, \quad (14)$$

$$\boldsymbol{\beta} = [\beta_1, \dots, \beta_N]^T. \quad (15)$$

By stacking the received echo signals at each BS as $\mathbf{y} = [\mathbf{y}_1^H, \dots, \mathbf{y}_N^H]^H$, we can equivalently get the following expression:

$$\mathbf{y} = \mathbf{A}(\boldsymbol{\theta}, \boldsymbol{\beta}) \odot \mathbf{B}(\boldsymbol{\alpha}) \mathbf{P} \mathbf{s} + \mathbf{n}, \quad (16)$$

where $\mathbf{A}(\boldsymbol{\theta}, \boldsymbol{\beta}) \in \mathbb{C}^{NL \times NL}$ and $\mathbf{B}(\boldsymbol{\alpha}) \in \mathbb{C}^{NL \times NL}$ are given by

$$\mathbf{A}(\boldsymbol{\theta}, \boldsymbol{\beta}) = [\mathbf{a}_r^H(\theta_1, \beta_1), \dots, \mathbf{a}_r^H(\theta_N, \beta_N)]^H \mathbf{A}_t(\boldsymbol{\theta}, \boldsymbol{\beta}), \quad (17)$$

$$\mathbf{B}(\boldsymbol{\alpha}) = [\boldsymbol{\alpha}_1, \dots, \boldsymbol{\alpha}_N]^T \otimes \mathbf{I}_L. \quad (18)$$

C. Performance Bound for Cooperative Localization

In this subsection, we introduce the SPEB to evaluate the performance of cooperative localization. SPEB is a lower bound of mean square error for any unbiased estimator $\hat{\mathbf{t}}$ of position \mathbf{t} [21], and can be calculated through

$$\mathbb{E} \left\{ (\hat{\mathbf{t}} - \mathbf{t}) (\hat{\mathbf{t}} - \mathbf{t})^T \right\} \geq \text{SPEB}(\mathbf{P}; \mathbf{t}) = \text{tr}(\mathbf{J}^{-1}(\mathbf{P}; \mathbf{t})), \quad (19)$$

where \mathbf{J} denotes the Fisher information matrix (FIM) for position parameter \mathbf{t} and \mathbf{P} is the joint beamforming matrix to be optimized. Based on [7], \mathbf{J} can be obtained by firstly calculating the equivalent FIM of angular parameters $\boldsymbol{\omega} = [\boldsymbol{\theta}^T, \boldsymbol{\beta}^T]^T$, denoted by $\mathbf{J}_e(\mathbf{P}; \boldsymbol{\omega})$, then transforming it to the FIM of position by multiplying both sides of $\mathbf{J}_e(\mathbf{P}; \boldsymbol{\omega})$ with the Jacobian matrix. Specifically, $\mathbf{J}_e(\mathbf{P}; \boldsymbol{\omega})$ can be calculated by

$$\mathbf{J}_e(\mathbf{P}; \boldsymbol{\omega}) = \frac{2}{\sigma^2} \text{Re} \left\{ \bar{\mathbf{P}}_s^H \mathbf{D}^H \Pi_{\tilde{\mathbf{A}}}^\perp \mathbf{D} \bar{\mathbf{P}}_s + \sum_{k=1}^K \bar{\mathbf{P}}_c^H \mathbf{D}^H \Pi_{\tilde{\mathbf{A}}}^\perp \mathbf{D} \bar{\mathbf{P}}_c \right\}, \quad (20)$$

where the components of (20) are expressed as

$$\Pi_{\tilde{\mathbf{A}}}^\perp = \mathbf{I} - \tilde{\mathbf{A}} (\tilde{\mathbf{A}}^H \tilde{\mathbf{A}})^{-1} \tilde{\mathbf{A}}^H \in \mathbb{C}^{NL \times NL}, \quad (21)$$

$$\tilde{\mathbf{A}} = (\mathbf{1}_{N^2}^T \otimes \mathbf{A}) \odot \frac{\partial \mathbf{B}}{\partial \boldsymbol{\alpha}} \in \mathbb{C}^{NL \times N^3 L}, \quad (22)$$

$$\frac{\partial \mathbf{B}}{\partial \boldsymbol{\alpha}} = \left[\frac{\partial \mathbf{B}}{\partial \alpha_{11}}, \dots, \frac{\partial \mathbf{B}}{\partial \alpha_{1N}}, \dots, \frac{\partial \mathbf{B}}{\partial \alpha_{NN}} \right], \quad (23)$$

$$\bar{\mathbf{P}}_s = \mathbf{I}_{2N} \otimes \mathbf{p}^s \in \mathbb{C}^{2N^2 L \times 2N}, \quad (24)$$

$$\bar{\mathbf{P}}_k = \mathbf{I}_{2N} \otimes \mathbf{p}_k^c \in \mathbb{C}^{2N^2 L \times 2N}. \quad (25)$$

$\mathbf{D} = [\mathbf{D}_\theta, \mathbf{D}_\beta] \in \mathbb{C}^{NL \times 2N^2L}$ in (20) is the partial derivative matrix with respect to ω . \mathbf{D}_θ and \mathbf{D}_β are respectively given by

$$\mathbf{D}_\theta = \left[\frac{\partial \mathbf{A}}{\partial \theta_1} \odot \mathbf{B}, \dots, \frac{\partial \mathbf{A}}{\partial \theta_N} \odot \mathbf{B} \right], \quad (26)$$

$$\mathbf{D}_\beta = \left[\frac{\partial \mathbf{A}}{\partial \beta_1} \odot \mathbf{B}, \dots, \frac{\partial \mathbf{A}}{\partial \beta_N} \odot \mathbf{B} \right]. \quad (27)$$

We further derive the FIM of position \mathbf{t} by

$$\mathbf{J}(\mathbf{P}; \mathbf{t}) = \mathbf{Q}^T \mathbf{J}_e(\mathbf{P}; \omega) \mathbf{Q}, \quad (28)$$

where \mathbf{Q} is given by

$$\mathbf{Q} = \frac{\partial \omega}{\partial \mathbf{t}} = \left[\frac{\partial \theta^T}{\partial \mathbf{t}}, \frac{\partial \beta^T}{\partial \mathbf{t}} \right]^T, \quad (29)$$

with

$$\frac{\partial \theta_n}{\partial \mathbf{t}} = \left[-\frac{(t_x - b_x^n)(t_z - b_z)}{d_{xy}^2 d_{xy}^n}, -\frac{(t_y - b_y^n)(t_z - b_z)}{d_{xy}^2 d_{xy}^n}, \frac{(d_{xy}^n)^2}{d_{xy}^2 d_{xy}^n} \right], \quad (30)$$

and

$$\frac{\partial \beta_n}{\partial \mathbf{t}} = \left[\frac{b_y^n - t_y}{(d_{xy}^n)^2}, \frac{t_x - b_x^n}{(d_{xy}^n)^2}, 0 \right]. \quad (31)$$

$d_{xy}^n = \sqrt{(b_x^n - t_x)^2 + (b_y^n - t_y)^2}$ denotes the Euclidean distance from the n -th BS to the sensing target on the x-y plane. The computational details can be found in Appendix A.

D. Problem Formulation

To achieve the optimal trade-off between the localization performance and communication performance in the CoISAC system, we maximize the total sum-rate of K communication users under the constraints for localization accuracy and total power by optimizing the joint beamforming vectors:

$$\max_{\mathbf{P}} \sum_{k=1}^K R_k \quad (32a)$$

$$s.t. \|\mathbf{p}_n^s\|_2^2 + \sum_{k=1}^K \|\mathbf{p}_{n,k}^c\|_2^2 \leq P_n, \forall n = 1, \dots, N \quad (32b)$$

$$\text{SPEB}(\mathbf{P}; \mathbf{t}) \leq \gamma, \quad (32c)$$

where γ is the predefined threshold for SPEB. In problem (32), constraint (32b) ensures the transmit power limitation of each BS. Constraint (32c) guarantees the target localization performance. Problem (32) is a highly non-convex problem. Traditional optimization methods rely on a series of convex approximation techniques to iteratively search for a sub-optimal solution, which can induce significant communication delays and unreliable performance in practical systems.

It can be seen that the optimization of beamforming vectors depends on the CSI of each communication user, i.e., \mathbf{h}_k , $\forall k \in \mathcal{K}$, through the communication data rate R_k , and the position of the target, i.e., \mathbf{t} , through the SPEB. Although there are many mature channel estimation algorithms in communication field and positioning algorithms in sensing field,

the channel $\hat{\mathbf{h}}$ and position $\hat{\mathbf{t}}$ obtained by the BSs inevitably suffer from estimation errors, i.e., $\hat{\mathbf{h}} = \mathbf{h} + \Delta \mathbf{h}$, $\hat{\mathbf{t}} = \mathbf{t} + \Delta \mathbf{t}$. Therefore, it is critical to consider robust beamforming design with the presence of the uncertainties of channel and position. There have been some standardized optimization techniques to address the parameter uncertainties, such as Robust Optimization (RO) for bounded error model [22] and Stochastic Programming (SP) for Gaussian error model [23]. However, these methods rely on idealized uncertainty model and often lead to increased algorithm complexity. Therefore, it is crucial to design more efficient, robust and scalable beamforming algorithms in CoISAC systems.

III. COOPERATIVE BEAMFORMING IN COISAC SYSTEMS BASED ON LHGNN

In this section, we model the CoISAC system using heterogeneous graphs, where different types of links are modeled as different types of nodes in graph data to effectively capture the heterogeneous topology and complex interactions of CoISAC systems. Then we introduce the detailed LHGNN architecture as well as the loss function to address the joint beamforming optimization problem in a data-driven manner. Let $\mathcal{Z} = \{1, \dots, Z\}$ denote the indices of sensing targets. For simplicity, the problem formulation in Section II-D assumes a single sensing target, i.e., $Z = 1$. However, the proposed algorithm can be easily extended to a multi-target sensing scenario. Therefore, we present the algorithm for a general multi-target system, with subscripts involving the target index z omitted when $Z = 1$.

A. Heterogeneous Graph Modeling of the CoISAC Systems

Heterogeneous graph data can typically be represented as $\mathcal{G} = (\mathcal{V}, \mathcal{E}, \mathcal{O}, \mathcal{R})$, where \mathcal{V} denotes the set of nodes in the graph data, \mathcal{E} represents the set of edges, and sets \mathcal{O} and \mathcal{R} represent the types of nodes and edges, respectively. In the modeling of the CoISAC system as heterogeneous graph data, we consider a more general scenario, wherein the modeled system includes N base stations, K communication users, and Z sensing targets.

1) *Heterogeneous Node*: When generating the node set \mathcal{V} , two types of nodes are constructed, i.e., $\mathcal{O} = \{o_c, o_s\}$, where o_c denotes the communication type, and o_s denotes the sensing type, respectively. To fully capture the heterogeneous nature of CoISAC systems, we propose an innovative approach that consolidates different link types in CoISAC into corresponding node types in the graph modeling. Specifically, there are NK communication links, each indexed by (n, k) , representing the communication link between BS n and communication user k . Additionally, there are NZ sensing links, each indexed by (n, z) , representing the sensing link between BS n and sensing target z . The communication links $\{(n, k), \forall n \in \mathcal{N}, k \in \mathcal{K}\}$ are modeled as communication type nodes, and the sensing links $\{(n, z), \forall n \in \mathcal{N}, z \in \mathcal{Z}\}$ are modeled as sensing type nodes. The total set of node indices $\mathcal{V} = \{1, 2, \dots, NK + NZ\}$ contains NK communication type nodes and NZ sensing type nodes. The mapping between a link (n, k) (or (n, z)) and its corresponding node index $v \in \mathcal{V}$

is represented by function φ , such that $\varphi(n, \cdot) = v$, with the inverse mapping given by $\varphi(v)^{-1} = (n, \cdot)$.

2) *Heterogeneous Edge*: When generating the edge set \mathcal{E} for the heterogeneous graph data, neighbor nodes are constructed separately for the two node types, i.e., o_c and o_s , thereby completing the construction of the edge set. The set of neighboring nodes for node $v \in \mathcal{V}$ is defined as

$$\mathcal{N}(v) = \{j \in \mathcal{V} : (v, j) \in \mathcal{E}\}. \quad (33)$$

Next, we will explain how to construct the neighboring nodes based on the type of the central node.

For a central node $\varphi(n, k)$ of type o_c , its connections to neighbor nodes include three different types of edges, namely $\mathcal{R}_c = \{r_{BS-CC}, r_{UE}, r_{BS-CS}\}$. If a neighbor node of type o_c shares the same base station with the central node, the edge connecting them is of type r_{BS-CC} . If a neighbor node of type o_c shares the same communication user with the central node, the edge connecting them is of type r_{UE} . If a neighbor node of type o_s shares the same base station with the central node, the edge connecting them is of type r_{BS-CS} . Define $\text{type}(\cdot)$ as the mapping from an edge $e \in \mathcal{E}$ to an edge type $r \in \mathcal{R}$. The construction of these three types of edges can be summarized by the following three expressions:

$$e = (\varphi(n, k), \varphi(n, k')), \text{type}(e) = r_{BS-CC}, \quad (34)$$

$$e = (\varphi(n, k), \varphi(n', k)), \text{type}(e) = r_{UE}, \quad (35)$$

$$e = (\varphi(n, k), \varphi(n, z)), \text{type}(e) = r_{BS-CS}. \quad (36)$$

Therefore, three different types of neighbor node sets for the central node $\varphi(n, k) = v$ can be represented as $\mathcal{N}_{BS-CC}(v)$, $\mathcal{N}_{UE}(v)$, and $\mathcal{N}_{BS-CS}(v)$, as shown in Fig. 4. These three neighbor sets satisfy the following properties:

$$\mathcal{N}_{BS-CC}(v) \cup \mathcal{N}_{UE}(v) \cup \mathcal{N}_{BS-CS}(v) = \mathcal{N}(v), \quad (37)$$

$$\mathcal{N}_{BS-CC}(v) \cap \mathcal{N}_{UE}(v) = \mathcal{N}_{BS-CC}(v) \cap \mathcal{N}_{BS-CS}(v)$$

$$= \mathcal{N}_{UE}(v) \cap \mathcal{N}_{BS-CS}(v) = \emptyset.$$

Each $\mathcal{N}_{BS-CC}(v)$ set contains $K - 1$ elements, each $\mathcal{N}_{UE}(v)$ set contains $N - 1$ elements, and each $\mathcal{N}_{BS-CS}(v)$ set contains Z elements, respectively. Therefore, each $\mathcal{N}(v)$ set contains $K + N + Z - 2$ elements, when v is of type o_c .

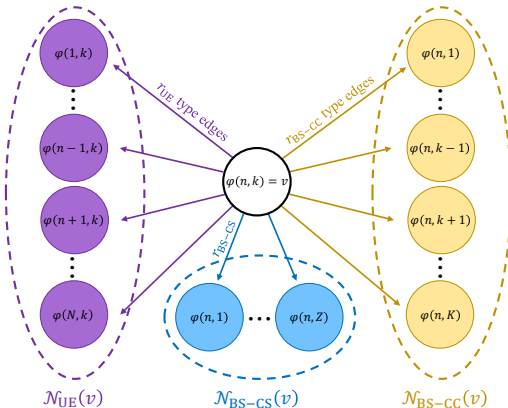


Fig. 4. A typical node of type o_c and its three types of neighbors.

For a central node $\varphi(n, z)$ of type o_s , the connections to its neighbor nodes also include three different types of edges, namely $\mathcal{R}_s = \{r_{BS-SS}, r_{TGT}, r_{BS-SC}\}$. If a neighbor node of type o_s shares the same base station with the central node, the edge connecting them is of type r_{BS-SS} . If a neighbor node of type o_s shares the same sensing target with the center node, the edge connecting them is of type r_{TGT} . If a neighbor node of type o_c shares the same BS with the central node, the edge connecting them is of type r_{BS-SC} . The construction of these three types of edges can be summarized as

$$e = (\varphi(n, z), \varphi(n, z')), \text{type}(e) = r_{BS-SS}, \quad (38)$$

$$e = (\varphi(n, z), \varphi(n', z)), \text{type}(e) = r_{TGT}, \quad (39)$$

$$e = (\varphi(n, z), \varphi(n, k)), \text{type}(e) = r_{BS-SC}. \quad (40)$$

Therefore, the three types of neighbor node sets for the central node $\varphi(n, z) = v'$ can be represented as $\mathcal{N}_{BS-SS}(v')$, $\mathcal{N}_{TGT}(v')$ and $\mathcal{N}_{BS-SC}(v')$, as shown in Fig. 5. These three neighbor sets satisfy the following properties:

$$\mathcal{N}_{BS-SS}(v') \cup \mathcal{N}_{TGT}(v') \cup \mathcal{N}_{BS-SC}(v') = \mathcal{N}(v'), \quad (41)$$

$$\begin{aligned} \mathcal{N}_{BS-SS}(v') \cap \mathcal{N}_{TGT}(v') &= \mathcal{N}_{BS-SS}(v') \cap \mathcal{N}_{BS-SC}(v') \\ &= \mathcal{N}_{TGT}(v') \cap \mathcal{N}_{BS-SC}(v') = \emptyset, \end{aligned} \quad (42)$$

Each $\mathcal{N}_{BS-SS}(v')$ set contains $Z - 1$ elements, each $\mathcal{N}_{TGT}(v')$ set contains $N - 1$ elements, and each $\mathcal{N}_{BS-SC}(v')$ set contains K elements, respectively. Therefore, each $\mathcal{N}(v')$ set contains $K + N + Z - 2$ elements, when node v' is of type o_s .

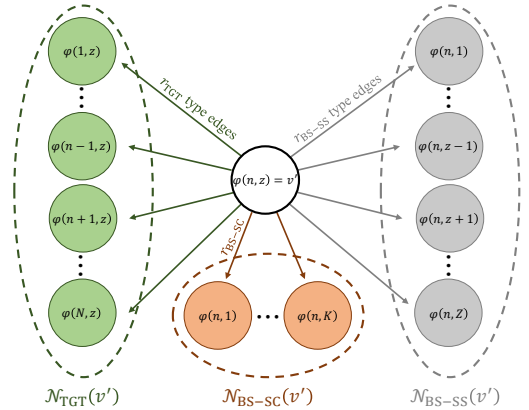


Fig. 5. A typical node of type o_s and its three types of neighbors.

Note that the construction of different types of edges in the graph depends on the joint beamforming design problem (32) in the CoISAC systems. For example, due to the per-BS power constraints, the performance of the communication and sensing links connected to the same BS is mutually constrained. Meanwhile, in the expressions of communication rate (4) and sensing SPEB (19), the communication beams and sensing beams transmitted from the same BS exhibit complex interactions, such as interference or mutual enhancement, leading to performance trade-offs between communication and sensing links associated with the same BS. Consequently, it is necessary to construct the edge types, such as r_{BS-CC} , r_{BS-CS} , r_{BS-SS} and r_{BS-SC} , to model these interactions. Furthermore, in the CoISAC systems, multi-BS cooperation

enables collaborative communication with the same user and joint positioning of the same target, thereby enhancing the communication and sensing performance. This requires the construction of r_{UE} and r_{TGT} types of edges to reflect such cooperative relationships. **Heterogeneous Graph**

For a CoISAC system with N BSs, K users, and Z sensing targets, a heterogeneous graph structure can be constructed using the aforementioned methods. This heterogeneous graph contains NK o_c -type nodes and NZ o_s -type nodes. Each o_c -type node is connected to its $K + N + Z - 2$ neighbor nodes through three types of edges, i.e., $\{r_{\text{BS-CC}}, r_{\text{UE}}, r_{\text{BS-CS}}\}$, while each o_s -type node is connected to its $K + N + Z - 2$ neighbor nodes through three types of edges, i.e., $\{r_{\text{BS-SS}}, r_{\text{TGT}}, r_{\text{BS-SC}}\}$. Note that when there is only one sensing target, edges of type $r_{\text{BS-SS}}$ will not exist. In the next subsection, we will explain how to perform learning over the constructed heterogeneous graph.

B. Framework of Attention-Enhanced LHGNN

The LHGNN performs learning on the proposed heterogeneous graph by leveraging information from neighbor nodes to enrich individual node features and propagating these features throughout the graph following its structured connections. Integrating an attention mechanism into the LHGNN introduces learnable weights during information aggregation, thereby enhancing the robustness of the network to the input data errors. In this subsection, we will provide a detailed introduction to the proposed LHGNN architecture enhanced by attention mechanism, comprising four components as shown in Fig. 6: an input layer, U GNN hidden layers, U' fully connected hidden layers, and an output layer with normalization operation. The input layer is utilized for embedding the input data, followed by the GNN hidden layers, which aggregate and update node features across the heterogeneous graph. During this process, an attention mechanism is employed to effectively and robustly extract the features based on the topological structure of CoISAC systems. The fully connected hidden layers learn the mapping between the graphical features and the joint beamforming vector for each link. Finally, the output layer generates the joint beamforming vectors corresponding to each link node.

1) *Input Layer*: In the input layer, initial node features are constructed for nodes of type o_c representing communication links and nodes of type o_s representing sensing links. These features serve as the input data for the GNN. For node $i = \varphi(n, k), \forall n \in \mathcal{N}, k \in \mathcal{K}$ of type o_c , the CSI $\mathbf{h}_{n,k}$ of the corresponding link (n, k) is used as the initial node feature. Therefore, the initial feature \mathbf{s}_i^0 for node i corresponding to communication link (n, k) is:

$$\mathbf{s}_i^0 = [\text{Re}(\mathbf{h}_{k,n}), \text{Im}(\mathbf{h}_{k,n})]^T \in \mathbb{R}^{2L \times 1}. \quad (43)$$

For node $i = \varphi(n, z), \forall n \in \mathcal{N}, z \in \mathcal{Z}$ of type o_s , the transmit steering vector $\mathbf{a}_t(\theta_{n,z}, \beta_{n,z})$ of the corresponding link (n, z) is used as the initial node feature, as shown in equation (8), where the elevation angle $\theta_{n,z}$ and azimuth angle $\beta_{n,z}$ are related to the position \mathbf{t}_z of the target z through the

geometric relationships. Therefore, the initial feature \mathbf{s}_i^0 for node i corresponding to sensing link (n, z) is:

$$\mathbf{s}_i^0 = [\text{Re}(\mathbf{a}_t(\theta_{n,z}, \beta_{n,z})), \text{Im}(\mathbf{a}_t(\theta_{n,z}, \beta_{n,z}))]^T \in \mathbb{R}^{2L \times 1}. \quad (44)$$

Note that the initial node features depend on the CSI of communication links and the position of sensing target, which can suffer from estimation errors. Therefore, during training, the input data for the network are the noisy CSI estimates $\hat{\mathbf{h}}_{k,n}$ and the noisy angles $\hat{\theta}_{n,z}$ and $\hat{\beta}_{n,z}$, such that the network can automatically learn how to mitigate the impact of input parameter errors during graphical feature extraction and beamforming learning, thus improving the robustness of the network.

2) *GNN Hidden Layer*: In the U GNN hidden layers, the network aggregates and updates feature information between neighboring nodes based on the constructed heterogeneous graph data, effectively utilizing topological information. Due to heterogeneity, different neural networks are used for feature mapping for different types of nodes and edges during the feature aggregation. To boost the robustness of the proposed method against estimation errors, an attention mechanism is introduced. The feature update process for the i -th node of type o_c in the u -th GNN hidden layer is represented as follows:

$$\begin{aligned} \mathbf{c}_i^{u+1} &= \frac{1}{|\mathcal{N}(i)|} \sum_{j \in \mathcal{N}(i)} \text{Norm}(\mathcal{F}_j^{u+1}) \in \mathbb{R}^{L^{u+1} \times 1}, \\ \mathbf{c}_i^{u+1} &= \frac{1}{|\mathcal{R}_c|} \sum_{r_\bullet \in \mathcal{R}_c} \text{Norm}(\mathcal{F}_{r_\bullet}^{u+1}) \in \mathbb{R}^{L^{u+1} \times 1}, \end{aligned} \quad (45)$$

where $\mathcal{R}_c = \{r_{\text{BS-CC}}, r_{\text{UE}}, r_{\text{BS-CS}}\}$ represents the set of different types of edges for nodes of type o_c , $\text{Norm}(\cdot)$ represents the normalization function layer, L^{u+1} denotes the dimension of the feature \mathbf{c}_i^{u+1} for node i after the update, and $\mathcal{F}_{r_\bullet}^{u+1}$ represents the aggregated features of type r_\bullet connecting edges, calculated as follows:

$$\mathcal{F}_{r_\bullet}^{u+1} = f_{\bullet}^{1,u}(\mathbf{c}_i^u) + \frac{1}{|\mathcal{N}_\bullet(i)|} \sum_{j \in \mathcal{N}_\bullet(i)} \lambda_{\bullet}^{u+1}(i, j) \times f_{\bullet}^{2,u}(\mathbf{c}_j^u). \quad (46)$$

When $\bullet = \text{BS} - \text{CS}$, the features of neighbor nodes to be aggregated in eq. (46) should be changed from \mathbf{c}_j^u to \mathbf{s}_j^u . The function $f(\cdot)$ represents a fully connected layer. Different fully connected networks (FCN) are used for different hidden GNN layers and for different edge types. The attention coefficient λ is calculated as follows:

$$\lambda_{\bullet}^{u+1} = \frac{\langle f_{\bullet}^3(\mathbf{c}_i^u), f_{\bullet}^4(\mathbf{c}_j^u) \rangle}{\sum_{j' \in \mathcal{N}_\bullet(i)} \langle f_{\bullet}^3(\mathbf{c}_i^u), f_{\bullet}^4(\mathbf{c}_{j'}^u) \rangle}, \quad (47)$$

where $\langle \mathbf{x}, \mathbf{y} \rangle = \exp\left(\frac{\mathbf{x}^T \mathbf{y}}{l}\right)$ represents the exponential scaled dot product [24], and l is the dimension of the vector. In expression (47), $l = L^{u+1}$. Similarly, when $\bullet = \text{BS} - \text{CS}$, \mathbf{c}_j^u in this expression should be replaced with \mathbf{s}_j^u . The introduction of the attention mechanism allows each node to focus on a subset of its neighbors, rather than considering all neighbors equally. Additionally, with learnable attention coefficients, the

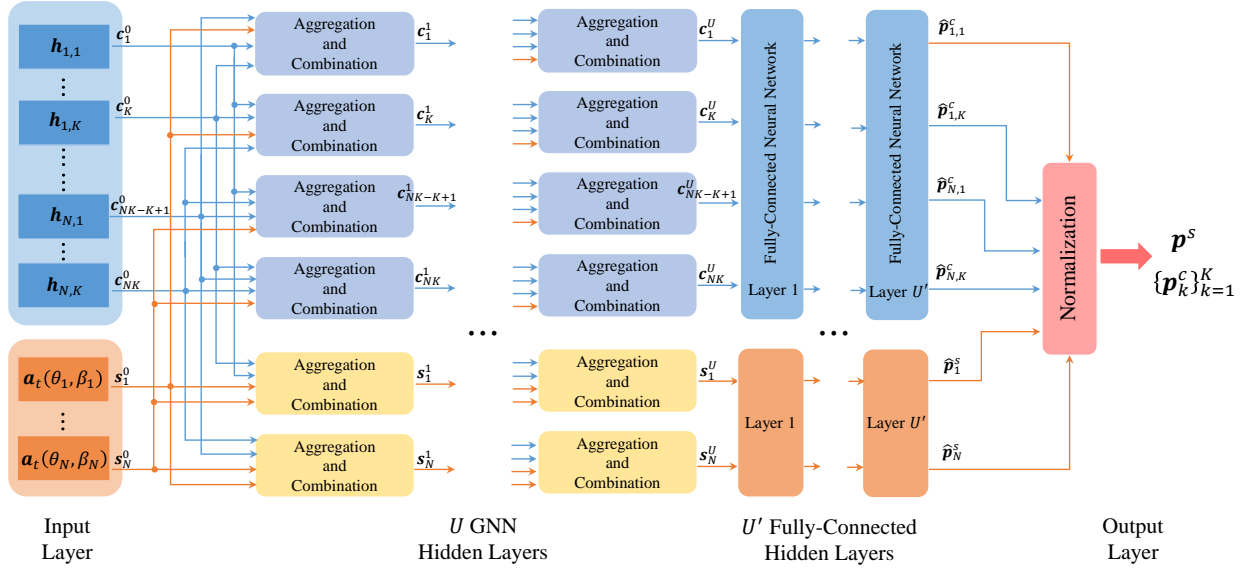


Fig. 6. The overall structure of the proposed heterogeneous graph neural network.

aggregation process can assign greater weight to neighbors that are more significant in the beamforming design, thus enabling the model to have certain robustness to noise in the initial node features. Similarly, the feature update process for the i -th node of type o_s in the u -th GNN hidden layer can be represented as

$$s_i^{u+1} = \frac{1}{|\mathcal{R}_s|} \sum_{r_\bullet \in \mathcal{R}_s} \text{Norm}(\mathcal{P}_{r_\bullet}^{u+1}) \in \mathbb{R}^{L^{u+1} \times 1}, \quad (48)$$

where $\mathcal{R}_s = \{r_{\text{TGT}}, r_{\text{BS-SC}}, r_{\text{BS-SS}}\}$ represents the set of different types of edges for nodes of type o_s , $\bullet \in \{\text{TGT}, \text{BS-SC}, \text{BS-SS}\}$, and $\mathcal{P}_{r_\bullet}^{u+1}$ represents the aggregated features of type r_\bullet connecting edges:

$$\mathcal{P}_{r_\bullet}^{u+1} = f_\bullet^1(s_i^u) + \frac{1}{|\mathcal{N}_\bullet(i)|} \sum_{j \in \mathcal{N}_\bullet(i)} \lambda_\bullet^{u+1}(i, j) \times f_\bullet^2(s_j^u). \quad (49)$$

When $\bullet = \text{BS-SC}$, features s_j^u in eq.(49) should be replaced by c_j^u . After feature aggregation and updating on U LHGNN hidden layers, feature vectors c_i^U and s_i^U containing the topological structure information in the heterogeneous graph are obtained at the output of the U -th hidden layer.

3) *Fully-Connected Hidden Layers*: U' fully connected hidden layers are utilized to learn the relationship between the feature vectors c_i^U and s_i^U and the beamforming vectors of the corresponding links. At the output of the U' -th fully connected hidden layer, the real and imaginary parts of the communication and sensing beamforming vectors corresponding to each node's link are obtained. These are then converted to complex numbers to obtain the joint beamforming matrix \mathbf{P} required to be solved in the optimization problem (32a). Specifically:

- For node $i = \varphi(n, k)$ of type o_c , the corresponding communication beamforming vector $\hat{p}_{n,k}^c$ from the n -th base station to the k -th user can be obtained through $[\text{Re}(\hat{p}_{n,k}^c), \text{Im}(\hat{p}_{n,k}^c)]^T =$

$FL_c(c_i^U; W_c^{(1)}, b_c^{(1)}, \dots, W_c^{(U')}, b_c^{(U')})$, where $FL_c(\cdot)$ denotes the composite function of the fully connected neural network for feature vector c_i^U , and W_c and b_c denote the weight matrix and bias of each layer in the network, respectively.

- For node $i = \varphi(n, z)$ of type o_s , the corresponding sensing beamforming vector $\hat{p}_{n,z}^s$ from the n -th base station to the z -th sensing target can be obtained through $[\text{Re}(\hat{p}_{n,z}^s), \text{Im}(\hat{p}_{n,z}^s)]^T = FL_s(s_i^U; W_s^{(1)}, b_s^{(1)}, \dots, W_s^{(U')}, b_s^{(U')})$, where $FL_s(\cdot)$ denotes the composite function of the fully connected neural network for feature vector s_i^U , and W_s and b_s denote the weight matrix and bias of each layer in the network, respectively.

4) *Output Layer*: At the output layer, a normalization operation is performed on the beamforming vectors $\hat{p}_{n,k}^c$ and $\hat{p}_{n,z}^s$ learned by the fully connected hidden layers. This ensures that the final output beamforming vectors $p_{n,k}^c$ and $p_{n,z}^s$ satisfy the power constraint in equation (32b). The specific normalization process is as follows:

$$p_{n,k}^c = \sqrt{P_n} \frac{\hat{p}_{n,k}^c}{\max(\sqrt{P_n}, \sqrt{\hat{P}_n})}, \quad (50a)$$

$$p_{n,z}^s = \sqrt{P_n} \frac{\hat{p}_{n,z}^s}{\max(\sqrt{P_n}, \sqrt{\hat{P}_n})}, \quad (50b)$$

$$\hat{P}_n = \sum_{z=1}^Z \|\hat{p}_{n,z}^s\|_2^2 + \sum_{k=1}^K \|\hat{p}_{n,k}^c\|_2^2. \quad (50c)$$

C. Loss Design of the LHGNN

In this subsection, we introduce the loss design of the LHGNN. An unsupervised learning approach is adopted to train the LHGNN, which enables the learning of the optimal beamforming vectors without labeled data. The literature [25] demonstrates that by introducing penalty terms, a constrained

optimization problem can be equivalently transformed into an unconstrained one. In the optimization problem (32a), power constraint (32b) has already been considered in the normalization operation at the output layer. Therefore, when designing the penalty term of the loss function, only constraint (32c) needs to be considered. Let the training dataset be $\{\mathbf{H}^i, \mathbf{A}_t^i(\boldsymbol{\theta}, \beta)\}_{i=1}^{I_T}$. The expression for the loss function is as follows:

$$\mathcal{L} = -\frac{1}{I_T} \sum_{i=1}^{I_T} \sum_{k=1}^K R_k^i \quad (51a)$$

$$+ \rho_1 \frac{1}{I_T} \sum_{i=1}^{I_T} [\max(0, \text{SPEB}^i - \gamma)] \quad (51b)$$

$$+ \rho_2 \frac{1}{I_T} \sum_{i=1}^{I_T} \sum_{k=1}^K [\max(0, r - R_k^i)]. \quad (51c)$$

The entire loss function can be divided into three parts. The first part is the negative of the objective function. By minimizing this part, we achieve the maximization of the achievable rate. The second part considers the constraint (32b), ensuring that the designed joint beamforming matrix can maximize the achievable rate while also guaranteeing the performance of sensing. The third part is a penalty term for local optimal solutions. Due to the highly non-convexity of the problem, the training of LHGNN can converge to bad local minima. To address this, a threshold is imposed on the per-user data rate during the model training to avoid some extreme local optima where the data rate is significantly low.

IV. SIMULATION RESULTS

In this section, simulation results are provided to demonstrate the effectiveness of the proposed cooperative beamforming algorithm based on LHGNN. We compare the sensing performance, communication performance, and robustness of the proposed algorithm with several benchmarks.

A. Parameter Settings

The simulation uses the "O1" outdoor scenario from the DeepMIMO dataset [26] to generate the required data, with the center frequency set to 28 GHz. The number of BSs is set to $N = 3$, using BSs with indices 1, 2, and 3 from the dataset. The coordinates of these three BSs are $\mathbf{b}^1 = [236, 390, 6]^T$, $\mathbf{b}^2 = [288, 390, 6]^T$, and $\mathbf{b}^3 = [236, 490, 6]^T$, respectively. Each BS is equipped with $L = L_x \times L_y = 16$ antennas, where $L_x = L_y = 4$. The system includes $K = 5$ single-antenna users. The coordinates of the target to be sensed are set to $\mathbf{t} = [244, 456, 22]$.

The unsupervised learning of the proposed LHGNN is completed using $I_T = 4000$ training data points. The LHGNN consists of $U = 9$ GNN hidden layers and $U' = 2$ fully connected hidden layers. In each GNN hidden layer, feature mapping, and attention coefficient learning are accomplished through fully connected networks. The output dimensions of features for different GNN hidden layers are as follows:

$$[2 \times L, 128, 128, 128, 256, 512, 256, 128, 2 \times L].$$

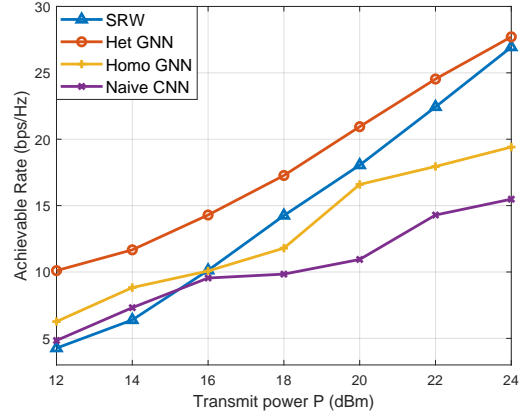


Fig. 7. Achievable rate versus transmit power of different algorithms.

In the loss function, the hyperparameters are set as $\rho_1 = 0.8 \times \text{epoch}$ and $\rho_2 = 0.5 \times \text{epoch}$ respectively, where epoch represents the current training round. The total number of training rounds is set to 800, and the threshold in the penalty term for local optimal solutions is set to $r = 0.05$. The model parameters of the network are updated and optimized by the Adam optimizer, with the initial learning rate set to 0.0002 and the weight decay coefficient set to 0.0005.

B. Benchmark Algorithms

To evaluate the performance of the proposed LHGNN in designing joint beamforming matrices, the following three methods are used as comparison benchmarks:

(1) *SRW* [7]: In this algorithm, an iterative algorithm based on SCA is designed to complete the joint beamforming matrix design. In the performance comparison, a strict constraint is set for SPEB to ensure a certain level of performance for the sensing task of the ISAC system.

(2) *Homo GNN*: In this algorithm, the heterogeneity of node and edge types is not considered. A homogeneous GNN is adopted, where the modeled graph data contains only one type of node and one type of edge. The design of the adjacency matrix and the initial node features are consistent with the proposed method. Similarly, a graph attention mechanism is also considered to automatically learn the aggregation priorities.

(3) *Naive CNN*: In this algorithm, convolutional neural networks (CNN) are adopted to extract features, and fully connected layers are then used to learn the mapping from features to joint beamforming. The input of the CNN is consistent with the initial node features of the proposed method.

When training the proposed algorithm, as well as Homo GNN and Naive CNN, unsupervised learning methods are adopted. The expression of the loss function is shown in equation (51), where the threshold γ for sensing performance is set to be the value of the SPEB result obtained after optimization by the SRW algorithm, such that all schemes are compared under the same sensing performance conditions.

C. Communication and Sensing Performance Evaluation

To evaluate the performance of different algorithms in terms of the communication metric of achievable rate, simulations

are conducted under different power constraint settings, as shown in Fig. 7. The results show that the achievable rates of all algorithms increase with the maximum transmission power. The proposed algorithm based on LHGNN can achieve better communication performance under different power constraints compared to other algorithms. Compared to the Naive CNN algorithm, both homogeneous and LHGNN algorithms achieve better performance. This indicates that by using GNN, features containing network topology information can be effectively extracted, thereby achieving better performance of joint beamforming. Compared to the Homo GNN algorithm, the performance gain of LHGNN comes from modeling the ISAC system using link heterogeneous graphs. The diversity of node types and the complicated interactions between communication links and sensing links during the optimization are better represented with heterogeneous graphs. Compared to the SRW algorithm, the proposed algorithm can achieve better communication performance under different transmission powers and shows greater performance gain when the maximum transmission power is smaller.

To verify the effectiveness of the loss function in guaranteeing the sensing performance, a further comparison of the SPEB under different maximum transmission power is conducted, as shown in Fig. 8. The threshold γ of sensing performance for the learning-based algorithms is set to the same optimized value as in SRW. The simulation results show that by using the designed loss function (51), the joint beamforming matrices learned by different neural networks can satisfy the constraint (32c) in the optimization problem. Therefore, the proposed algorithm can not only achieve good achievable rates but also ensure sensing performance.

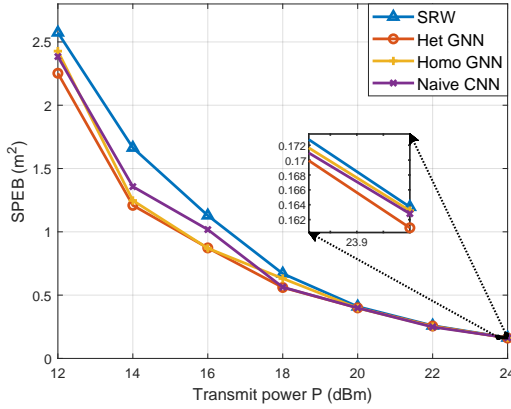


Fig. 8. SPEB versus transmit power of different algorithms.

D. Robustness Evaluation

Due to the difficulty of perfectly estimating channel parameters and the position parameters of sensing targets, the network inputs can contain a certain degree of estimation noise. Hence, it is necessary to further evaluate whether the designed network can exhibit certain robustness to estimation noises.

Let $\hat{\mathbf{h}}_{k,n}$ and $\hat{\mathbf{a}}_t(\hat{\theta}_n, \hat{\beta}_n)$ represent the noisy communication node features and sensing node features respectively. The error

of $\hat{\mathbf{h}}_{k,n}$ depends on the accuracy of channel estimation, which incorporates the signal-to-noise ratio (SNR). The noise in $\hat{\mathbf{a}}_t(\hat{\theta}_n, \hat{\beta}_n)$ comes from position error. Denote the estimated coordinates of the sensing target by $\hat{\mathbf{t}} = [\hat{t}_x, \hat{t}_y, \hat{t}_z]^T = [t_x + \Delta t_x, t_y + \Delta t_y, t_z + \Delta t_z]^T$, where Δt_x , Δt_y and Δt_z represent the position estimation errors in different dimensions. With estimated coordinates $\hat{\mathbf{t}}$, the angle estimation values $\hat{\theta}_n$ and $\hat{\beta}_n$ of the n -th BS can be calculated based on (5) and (6). Then we can calculate the noisy transmit steering vector $\hat{\mathbf{a}}_t(\hat{\theta}_n, \hat{\beta}_n)$ with estimated angles. Therefore, the noise level of the sensing node feature $\hat{\mathbf{a}}_t(\hat{\theta}_n, \hat{\beta}_n)$ can be measured by position estimation errors Δt_x , Δt_y and Δt_z . In the simulation process, the input data is modified to $\{\hat{\mathbf{H}}^i, \hat{\mathbf{A}}_t^i(\theta, \beta)\}_{i=1}^{I_T}$, while the noise-free dataset $\{\mathbf{H}^i, \mathbf{A}_t^i(\theta, \beta)\}_{i=1}^{I_T}$ is used for loss calculation. Other simulation settings remain the same. The results are shown in Fig. 9 and Fig. 10. The “LHGNN w/o attention” algorithm adopts the same LHGNN but does not use the attention mechanism, i.e., the aggregation process of this network only needs to average the feature values of all neighboring nodes, and other parameter settings are consistent with the proposed algorithm.

In Fig. 9, the impact of different levels of channel estimation error is evaluated, with the initial level of position estimation error set to $\Delta t_x, \Delta t_y, \Delta t_z \in [2, 3)$, meaning the coordinate estimation error is randomly generated from 2 to 3 meters. The maximum transmission power of each BS is set to $P = 20$ dBm. The simulation results show that the proposed algorithm can exhibit good robustness under different levels of channel estimation noise, achieving good performance even at $\text{SNR} = 0$ dB. Meanwhile, the simulation results indicate that introducing the attention mechanism can further enhance the robustness of LHGNN. The reason is that the attention mechanism allows the network to automatically learn attention coefficients during the aggregation process, thereby assigning smaller weight values to neighboring nodes severely contaminated by noise, resulting in better model robustness. In Homo GNN algorithm, although attention mechanisms are also used, the lack of heterogeneity in modeling makes it more susceptible to data noise and resulting in lower robustness.

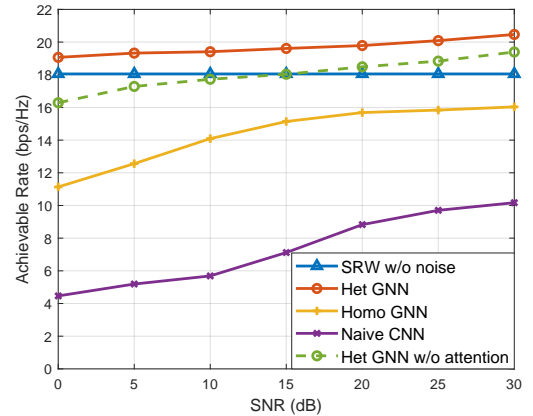


Fig. 9. Achievable rate versus SNR of different algorithms.

In Fig. 10, the impact of different levels of position error is evaluated, with the initial position SNR to be $\text{SNR} = 20$ dB,

and the transmission power to be $P = 20\text{dBm}$. The simulation results show that the proposed algorithm can exhibit good robustness to different levels of position estimation noise for sensing targets, achieving good performance even when the coordinate error $\Delta t_x, \Delta t_y, \Delta t_z \in [6, 7]$. Similarly, the proposed algorithm demonstrates the best robustness to position error. Therefore, by modeling network heterogeneity and incorporating an attention mechanism, the proposed algorithm significantly enhances the robustness of beamforming in CoISAC systems against the communication channel errors and sensing information errors.

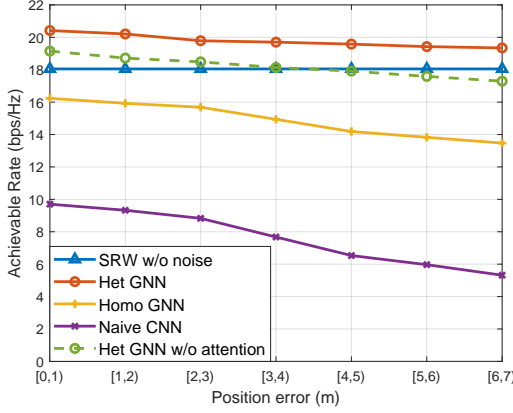


Fig. 10. Achievable rate versus position error of different algorithms.

V. CONCLUSIONS

In this paper, we investigate multi-BS collaborative localization and communication in CoISAC systems and introduce the LHGNN for joint beamforming design. By modeling different types of links as heterogeneous nodes and their interactions as edges, LHGNN effectively captures the structural dependencies within CoISAC networks, surpassing traditional bipartite graph models. To enhance robustness against channel and position estimation errors, we integrate a graph attention mechanism that dynamically adjusts node and link importance, mitigating the impact of inaccurate inputs. Numerical results validate that the proposed attention-enhanced LHGNN achieves superior communication rates while maintaining sensing performance under power constraints. Additionally, the proposed method demonstrates strong resilience to system uncertainties, highlighting its effectiveness in real-world CoISAC applications.

APPENDIX

A. Derivation of 20

The FIM w.r.t. unknown position-related parameters $\eta = [\omega^T, \alpha^T, \sigma^2]^T$ is

$$\mathbf{J}_\eta = \begin{bmatrix} \mathbf{J}_{\omega\omega} & \mathbf{J}_{\omega\alpha} & 0 \\ \mathbf{J}_{\omega\alpha}^T & \mathbf{J}_{\alpha\alpha} & 0 \\ 0 & 0 & NL/\sigma^4 \end{bmatrix},$$

where $[\mathbf{J}_{\omega\omega}]_{ij} \triangleq \frac{2}{\sigma^2} \text{Re} \left\{ \frac{\partial \mathbf{u}^H}{\partial \omega_i} \frac{\partial \mathbf{u}}{\partial \omega_j} \right\}$, $\mathbf{u} = (\mathbf{A} \odot \mathbf{B})\mathbf{P}\mathbf{s}$ and $\mathbf{J}_{\omega\alpha}$, $\mathbf{J}_{\alpha\alpha}$ are defined similarly. Note that we omit the sample

time t for derivation. Performing EFIM on angle parameter ω , we have

$$\mathbf{J}_e(\omega; \mathbf{P}) = \mathbf{J}_{\omega\omega} - \mathbf{J}_{\omega\alpha} \mathbf{J}_{\alpha\alpha}^{-1} \mathbf{J}_{\omega\alpha}^T. \quad (52)$$

Firstly, we calculate the derivatives of \mathbf{u} w.r.t. ω and α

$$\begin{aligned} \frac{\partial \mathbf{u}}{\partial \omega_i} &= \left(\frac{\partial \mathbf{A}}{\partial \omega_i} \odot \mathbf{B} \right) \mathbf{P}\mathbf{s}, i = 1, \dots, 2N, \\ \frac{\partial \mathbf{u}}{\partial \alpha_{u,n}} &= \left(\mathbf{A} \odot \frac{\partial \mathbf{B}}{\partial \alpha_{u,n}} \right) \mathbf{P}\mathbf{s}, \end{aligned}$$

where $\frac{\partial \mathbf{u}}{\partial \omega_i}$ and $\frac{\partial \mathbf{u}}{\partial \alpha_{u,n}}$ can be rewritten in a compact form

$$\frac{\partial \mathbf{u}}{\partial \omega_i} = \mathbf{D}\bar{\mathbf{P}}\bar{\mathbf{S}} \in \mathbb{C}^{NL \times 2N}, \frac{\partial \mathbf{u}}{\partial \alpha} = \tilde{\mathbf{A}}\ddot{\mathbf{P}}\ddot{\mathbf{S}} \in \mathbb{C}^{NL \times N^2}.$$

with $\tilde{\mathbf{A}} = (\mathbf{1}_{N^2}^T \otimes \mathbf{A}) \odot \frac{\partial \mathbf{B}}{\partial \alpha}$, $\ddot{\mathbf{P}} = \mathbf{I}_{N^2} \otimes \mathbf{P} \in \mathbb{C}^{N^3 L \times N^2(K+1)}$, $\ddot{\mathbf{S}} = \mathbf{I}_{N^2} \otimes \mathbf{s}$ and $\tilde{\mathbf{S}} = \mathbf{I}_{2N} \otimes \mathbf{s}$. Then, we obtain the FIM expressions as follows,

$$\begin{aligned} \mathbf{J}_{\omega\omega} &= \frac{2}{\sigma^2} \text{Re} \left\{ \bar{\mathbf{S}}^H \bar{\mathbf{P}}^H \mathbf{D}^H \mathbf{D} \bar{\mathbf{P}} \bar{\mathbf{S}} \right\}, \\ \mathbf{J}_{\omega\alpha} &= \frac{2}{\sigma^2} \text{Re} \left\{ \bar{\mathbf{S}}^H \bar{\mathbf{P}}^H \mathbf{D}^H \tilde{\mathbf{A}} \ddot{\mathbf{P}} \ddot{\mathbf{S}} \right\}, \\ \mathbf{J}_{\alpha\alpha} &= \frac{2}{\sigma^2} \text{Re} \left\{ \ddot{\mathbf{S}}^H \ddot{\mathbf{P}}^H \tilde{\mathbf{A}}^H \tilde{\mathbf{A}} \ddot{\mathbf{P}} \ddot{\mathbf{S}} \right\}. \end{aligned} \quad (53)$$

Using the fact $\mathbf{X}\mathbf{Y}(\mathbf{Y}^H \mathbf{X}^H \mathbf{X} \mathbf{Y})^\dagger \mathbf{Y}^H \mathbf{X}^H = \mathbf{X}(\mathbf{X}^H \mathbf{X})^\dagger \mathbf{X}^H = \Pi_{\mathbf{X}}^\perp$ where \mathbf{X} and \mathbf{Y} are full row and full column rank matrix, plugging (53) into (52), we obtain

$$\mathbf{J}_e(\omega; \mathbf{P}) = \frac{2}{\sigma^2} \text{Re} \left\{ \bar{\mathbf{S}}^H \bar{\mathbf{P}}^H \mathbf{D}^H \Pi_{\tilde{\mathbf{A}}}^\perp \mathbf{D} \bar{\mathbf{P}} \bar{\mathbf{S}} \right\}, \quad (54)$$

with

$$\begin{aligned} [\mathbf{J}_e(\omega; \mathbf{P})]_{ij} &= \mathbf{p}^{c,H} \mathbf{D}_i^H \Pi_{\tilde{\mathbf{A}}}^\perp \mathbf{D}_j \mathbf{p}^c \sum_{t=1}^T s_c s_c^* / T \\ &\quad + \sum_{k=1}^K \mathbf{p}_k^{p,H} \mathbf{D}_i^H \Pi_{\tilde{\mathbf{A}}}^\perp \mathbf{D}_j \mathbf{p}_k^p \sum_{t=1}^T s_k s_k^* / T, \\ &= \frac{2}{\sigma^2} \text{Re} \left\{ \left(\mathbf{p}^{c,H} \mathbf{D}_i^H \Pi_{\tilde{\mathbf{A}}}^\perp \mathbf{D}_j \mathbf{p}^c \right) \odot \Lambda_c \right. \\ &\quad \left. + \sum_{k=1}^K \left(\mathbf{p}_k^{p,H} \mathbf{D}_i^H \Pi_{\tilde{\mathbf{A}}}^\perp \mathbf{D}_j \mathbf{p}_k^p \right) \odot \Lambda_k \right\}, \end{aligned}$$

where t is sample time index and \mathbf{D}_i is the i -th block of \mathbf{D} . Since the covariance matrix of \mathbf{s} is identity matrix, we can obtain EFIM expression as in (20)

REFERENCES

- [1] D. K. P. Tan, J. He, Y. Li, A. Bayesteh, Y. Chen, P. Zhu, and W. Tong, "Integrated sensing and communication in 6G: Motivations, use cases, requirements, challenges and future directions," in *2021 1st IEEE International Symposium on Joint Communications & Sensing (JC&S)*. IEEE, 2021, pp. 1–6.
- [2] J. Wu, Z. Zhang, Y. Hong, and Y. Wen, "Cloud radio access network (C-RAN): a primer," *IEEE network*, vol. 29, no. 1, pp. 35–41, 2015.

- [3] A. Liu, L. Lian, V. Lau, G. Liu, and M.-J. Zhao, "Cloud-assisted cooperative localization for vehicle platoons: A turbo approach," *IEEE Transactions on Signal Processing*, vol. 68, pp. 605–620, 2020.
- [4] A. Liu, Z. Huang, M. Li, Y. Wan, W. Li, T. X. Han, C. Liu, R. Du, D. K. P. Tan, J. Lu *et al.*, "A survey on fundamental limits of integrated sensing and communication," *IEEE Communications Surveys & Tutorials*, vol. 24, no. 2, pp. 994–1034, 2022.
- [5] L. Chen, X. Qin, Y. Chen, and N. Zhao, "Joint waveform and clustering design for coordinated multi-point DFRC systems," *IEEE Trans. Commun.*, vol. 71, no. 3, pp. 1323–1335, 2023.
- [6] N. Babu, C. Masouros, C. B. Papadias, and Y. C. Eldar, "Precoding for multi-cell ISAC: from coordinated beamforming to coordinated multipoint and bi-static sensing," *arXiv preprint arXiv:2402.18387*, 2024.
- [7] P. Gao, L. Lian, and J. Yu, "Cooperative ISAC with direct localization and rate-splitting multiple access communication: A pareto optimization framework," *IEEE Journal on Selected Areas in Communications*, vol. 41, no. 5, pp. 1496–1515, 2023.
- [8] X. Yang, Z. Wei, J. Xu, Y. Fang, H. Wu, and Z. Feng, "Coordinated transmit beamforming for networked ISAC with imperfect CSI and time synchronization," *IEEE Transactions on Wireless Communications*, 2024.
- [9] H. Zhang, H. Sun, T. He, W. Xiang, and R. Q. Hu, "Energy efficient robust beamforming for vehicular ISAC with imperfect channel estimation," in *2024 IEEE International Conference on Communications Workshops (ICC Workshops)*. IEEE, 2024, pp. 1864–1869.
- [10] C. Liu, W. Yuan, S. Li, X. Liu, H. Li, D. W. K. Ng, and Y. Li, "Learning-based predictive beamforming for integrated sensing and communication in vehicular networks," *IEEE Journal on Selected Areas in Communications*, vol. 40, no. 8, pp. 2317–2334, 2022.
- [11] X. Liu, H. Zhang, K. Long, M. Zhou, Y. Li, and H. V. Poor, "Proximal policy optimization-based transmit beamforming and phase-shift design in an IRS-aided ISAC system for the thz band," *IEEE Journal on Selected Areas in Communications*, vol. 40, no. 7, pp. 2056–2069, 2022.
- [12] R. Yang, Z. Zhu, J. Zhang, S. Xu, C. Li, Y. Huang, and L. Yang, "Deep learning-based joint transmit beamforming for dual-functional radar-communication system," *IEEE Transactions on Wireless Communications*, 2024.
- [13] Q. Qi, X. Chen, C. Zhong, C. Yuen, and Z. Zhang, "Deep learning-based design of uplink integrated sensing and communication," *IEEE Transactions on Wireless Communications*, 2024.
- [14] X. Chen, Z. Feng, J. A. Zhang, F. Gao, X. Yuan, Z. Yang, and P. Zhang, "Complex CNN CSI enhancer for integrated sensing and communications," *IEEE Journal of Selected Topics in Signal Processing*, 2024.
- [15] P. Pulkkinen and V. Koivunen, "Model-based online learning for active ISAC waveform optimization," *IEEE Journal of Selected Topics in Signal Processing*, 2024.
- [16] Y. Shi, L. Lian, Y. Shi, Z. Wang, Y. Zhou, L. Fu, L. Bai, J. Zhang, and W. Zhang, "Machine learning for large-scale optimization in 6G wireless networks," *IEEE Communications Surveys & Tutorials*, 2023.
- [17] Y. Shen, J. Zhang, S. Song, and K. B. Letaief, "Graph neural networks for wireless communications: From theory to practice," *IEEE Transactions on Wireless Communications*, vol. 22, no. 5, pp. 3554–3569, 2022.
- [18] X. Yan, Z. Wang, Y. Jia, Z. Zhang, and Y. Huang, "Access point selection and beamforming design for cell-free network: From fractional programming to GNN," *IEEE Transactions on Wireless Communications*, 2024.
- [19] X. Li, M. Chen, Y. Hu, Z. Zhang, D. Liu, and S. Mao, "Jointly optimizing terahertz based sensing and communications in vehicular networks: A dynamic graph neural network approach," *IEEE Transactions on Wireless Communications*, 2024.
- [20] Z. Huang, Z. Wang, and S. Chen, "Sub-6GHz Assisted mmWave Hybrid Beamforming with Heterogeneous Graph Neural Network," *IEEE Transactions on Communications*, 2024.
- [21] H. Zhao, N. Zhang, and Y. Shen, "Beamspace direct localization for large-scale antenna array systems," *IEEE Transactions on Signal Processing*, vol. 68, pp. 3529–3544, 2020.
- [22] A. Ben-Tal, A. Nemirovski, and L. El Ghaoui, "Robust optimization," 2009.
- [23] A. Shapiro, D. Dentcheva, and A. Ruszczyński, *Lectures on stochastic programming: modeling and theory*. SIAM, 2021.
- [24] A. Vaswani, N. Shazeer, N. Parmar, J. Uszkoreit, L. Jones, A. N. Gomez, Ł. Kaiser, and I. Polosukhin, "Attention is all you need," *Advances in neural information processing systems*, vol. 30, 2017.
- [25] P. E. Gill, W. Murray, and M. H. Wright, *Practical optimization*. SIAM, 2019.
- [26] A. Alkhateeb, "DeepMIMO: A generic deep learning dataset for millimeter wave and massive MIMO applications," *arXiv preprint arXiv:1902.06435*, 2019.